Theoretical model for coupled dual impinging jet aeroacoustic resonance

Spencer L. Stahl [*] and Datta Gaitonde [†]
Mechanical and Aerospace Engineering, The Ohio State University, Columbus, Ohio 43210, USA

Vikas N. Bhargav [‡] and Farrukh S. Alvi [§]
Department of Mechanical Engineering, Florida State University, Tallahassee, Florida 32310, USA

(Received 14 April 2022; accepted 29 September 2022; published 14 October 2022)

A theoretical model is constructed to understand and predict the aeroacoustic feedback coupling of dual impinging jet (DIJ) configurations of the type encountered in supersonic vertical takeoff and landing aircraft. The proposed model extends the single impinging jet (SIJ) framework of Powell, which derives impinging tone frequencies from the speeds of downstream convecting features and upstream propagating acoustic waves generated by periodic ground impingement. The SIJ feedback mechanism dominates *each* jet, but fails to predict anomalous changes in acoustic characteristics due to the proximal second jet. The new DIJ model eliminates this shortcoming by introducing a third, acoustically coupled DIJ global feedback loop that augments the two individual SIJ loops. It is shown that the two principal length parameters, nozzle to ground (H) and internozzle separation (S) distances, can foster a synchronized *coresonance* condition in which the coupled global feedback loop interacts with preferred individual SIJ feedback modes. The occurrence of this coupled dynamic state is quantified by a coresonance factor R_{DIJ}, a metric from 0 to 1 that relates all three feedback loops in the DIJ system. We focus on a configuration where the coupling is primarily acoustic in nature, specifically, two identical underexpanded Mach 1.27 jets. Experimental and numerical simulations are used to calibrate the model inputs at select points in the parameter space, and predictions from the model are then shown to be generally applicable by comparisons with acoustic measurements at other conditions. In particular, the model successfully predicts the damping or amplification of SIJ impinging tones due to the influence of the second jet, as well as overall sound pressure level trends as a function of impingement height.

DOI: 10.1103/PhysRevFluids.7.104606

I. INTRODUCTION

Impinging jets produce strong tones due to aeroacoustic resonance established between the jet nozzle and the impingement surface (plate). The mechanism is generally described in terms of self-reinforcing feedback of downstream (towards the plate) convecting instabilities in the jet shear-layer and upstream (towards the nozzle) propagating acoustic waves outside the jet. This feedback loop is the dominant driver for subsonic and supersonic impinging jets alike, and it has been extensively studied for single impinging jets (SIJs), resulting in well accepted models based on the work of Powell [1,2].

[*]stahl.174@osu.edu
[†]gaitonde.3@osu.edu
[‡]vn16d@my.fsu.edu
[§]falvi@fsu.edu

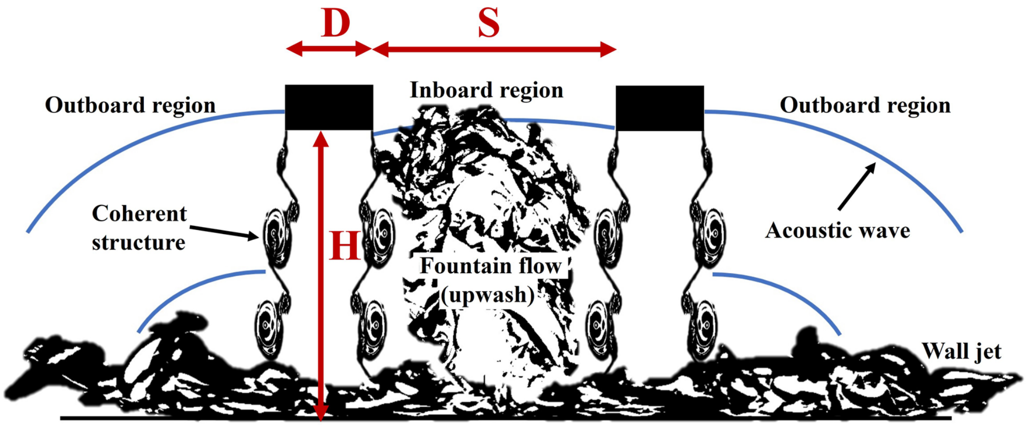

FIG. 1. Schematic of dual impinging jets showing primary flow features and geometric parameters. The resonance mechanism is comprised of downward traveling coherent structures in the jets and upward propagating acoustic waves. The outboard sides behave similarly to SIJs, while the inboard region experiences acoustic and hydrodynamic coupling effects.

Dual impinging jets (DIJs) are employed in many applications, such as vertical takeoff and landing (VTOL) aircraft. The two jets may be identical or dissimilar; regardless, their dynamics are significantly more complicated than SIJs, and they lead to anomalous acoustic behavior such as the strengthening or weakening of impinging tones [3,4]. The current work proposes an acoustically coupled DIJ feedback mechanism, which, in conjunction with the established SIJ feedback model of Powell, improves the prediction of resonance characteristics due to the presence of the second jet.

The parameters and jet dynamics of interest in the DIJ configuration are illustrated in Fig. 1. The geometric parameters are the height (H) of the nozzle exit from the plate, the diameter (D) of the nozzle, and the nozzle separation distance (S). The coupling mechanisms between jets in the DIJ configuration effectively modulate the self-resonance of each jet, which is summarized first by considering the physics of the simpler, more extensively examined SIJ case. The SIJ feedback loop is illustrated in Fig. 1 on the sides marked "outboard region," i.e., the domain relatively less influenced by the other jet. Briefly, the turbulent plume of the jet develops coherent structures through instability growth, found in classical [2] and more recent studies [5–7]. These structures impinge on the surface, and the flow is redirected radially in the wall-jet region [8,9]. Acoustic waves generated during the impingement process propagate back towards the nozzle exit to establish a feedback resonance, leading to the production of intense impinging tones, typically at least 10 dB above the broadband noise spectra [10,11]. Experiments using shadowgraph and particle image velocimetry (PIV) have tracked the coherent vortical structures in the shear layer and related their convection speeds to impinging tone frequencies [5,11]. This feedback is similar in many ways to that associated with "screech" tones observed in free jets containing shocks [12]. Underexpanded impinging jets at moderate heights may experience both screech and impinging tones. However, impingement resonance is more dominant at lower heights [13–15]. A recent review by Edgington-Mitchell [16] may be consulted for a comprehensive discussion of these resonance mechanisms.

The seminal model of Powell [2] has been widely adopted as the standard for predicting impingement tones. The four necessary components of the feedback loop are as follows [16]: (i) The *receptivity process* denoting the interaction of acoustic disturbances at the nozzle lip with the incipient shear layer, resulting in hydrodynamic Kelvin-Helmholtz (KH) instabilities. (ii) The *downstream process* referring to shear-layer convection and growth of these KH instabilities into coherent structures traveling downstream. (iii) The *sound generation process* by which acoustic wave sources are introduced at the plate, typically attributed to the impingement of coherent structures or unsteady standoff shock motion. (iv) The *upstream process* of acoustic disturbance propagation from the plate towards the lip of the nozzle. Resonance occurs when these feedback components are self-reinforcing, with suitable amplitude, phase, and gain. The periodicity of this process is essential to the genesis of the observed tones.

A simplified form of Powell's model predicts impinging tone frequencies based on the contributions of each process as

$$\frac{n}{F} = \frac{H}{U} + \frac{H}{a} + p, \quad n = 1, 2, 3, \ldots, \tag{1}$$

where the fundamental feedback loop frequency F and integer multiples n are related to the combined period of time for the downstream (H/U) and upstream (H/a) processes, along with a phase lag term p. While the spatially averaged shear-layer convection speed (U) and ambient speed of sound (a), representing downstream and upstream propagation, respectively, may be measured, the receptivity and sound generation components are accounted for in the phase lag term p in order to recover the observed acoustic tones. Typically, U is either estimated from an empirical function of nozzle exit velocity (dependent on jet operating conditions) or directly from the measured or computed flow-field [17]. Powell's formula has proven very successful in predicting impinging mode frequencies nF, but the relative amplitudes of the possible impinging tones are indeterminate. The SIJ mechanism also obviously does not account for any DIJ coupling, which affects the sound field and is the focus of this paper.

Returning to the qualitative picture of the DIJ flow field in Fig. 1, the "inboard" region comprises a complicated flow arising from the interaction of the wall-jets that form after impingement. The resulting fountain flow, or upwash, contains turbulent fluid in the region between the jets, ejecting plumes and coupling the jets [18]. Although the tonal SIJ feedback behavior persists, significant differences emerge between SIJ and DIJ aeroacoustic-resonance modes and acoustic spectra [4,19,20]. Whereas the individual jets contain axisymmetric or asymmetric impinging modes [15], globally, in-phase or out-of-phase impingement modes are found across both jets, and unique dynamics emerge due to the fountain-flow interactions [21].

The *hydrodynamic* coupling between the jets via the fountain flow is clearly very complex. The primary focus in this work, however, is on the *acoustic* coupling between the jets, which is facilitated by considering identical DIJ (IDIJ); these produce a symmetric (in the mean) fountain-flow with relatively minimal direct shear-layer interactions and weak hydrodynamic coupling [22–24]. Globally coupled IDIJ modes found in the schlieren imaging experiments of Wong [25] were also successfully detected in simulations [26], and they are attributed to acoustic coupling. Acoustic measurements demonstrate how such global modes can strengthen or weaken certain impinging tones in the individual jets [3,4]. The optimal impinging tone in the IDIJ system depends on the nozzle pressure ratio, impingement heights, and separation distance [27], but the exact relationship to the acoustic coupling phenomenon is not clear.

As an example of the acoustic coupling effects, Fig. 2 shows measurements from the "inner" microphone positioned in schematic (a), comparing two Mach 1.27 underexpanded (nozzle pressure ratio 2.65) jets under SIJ and DIJ configurations. The inner microphone better captures acoustic waves from both jets, while the outer microphone highlights directional differences in sound [4,28]. Figure 2(b) plots the overall sound pressure level (OASPL) across a range of impinging heights with free jet values shown for Ref. [4]. For both SIJs and DIJs, the impingement surface substantially increases OASPL at all heights compared to free jets. The SIJ case is initially louder than the DIJ case for $H/D < 6$; however, this trend reverses for larger heights where the OASPL asymptotically decays to free jet levels. The shapes of the SIJ and DIJ curves are nonlinear and quite different from each other, with the SIJ sound level peaking at $H/D = 4$, examined further in Sec. III. The acoustic spectra at this height are shown in Fig. 2(c) and demonstrate a relative decrease or increase to impinging tone amplitude in the DIJ configuration, as denoted by the red and green circles, respectively. The goal of this work is to develop a model that can predict the anomalous SIJ-DIJ

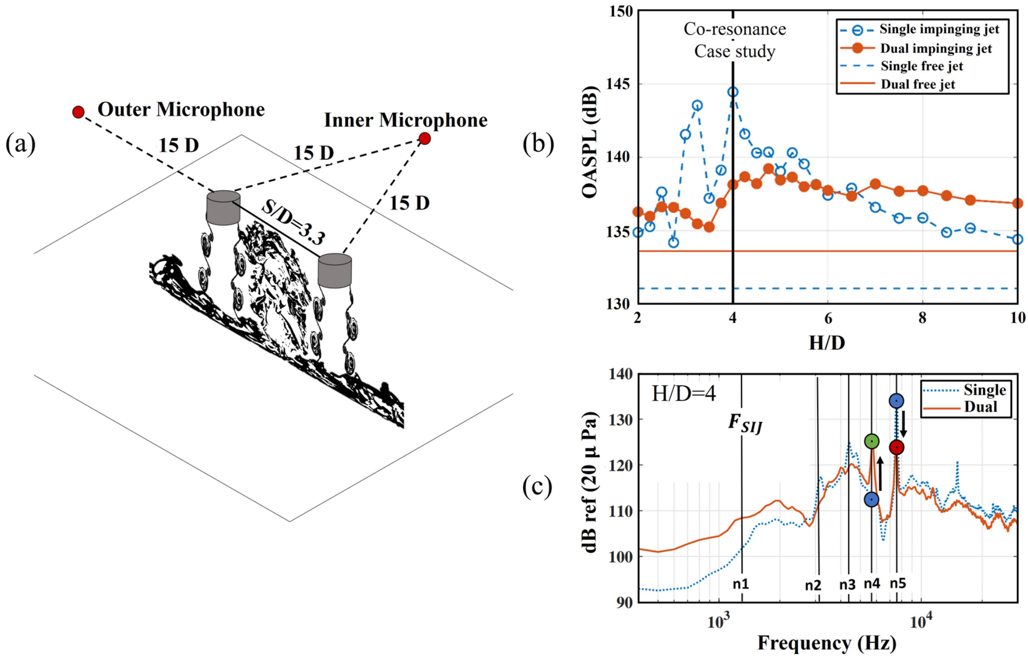

FIG. 2. Comparison of SIJ and DIJ acoustic characteristics for Mach 1.27 underexpanded (nozzle pressure ratio 2.65) jets. (a) The inner and outer microphone positions measured in nozzle diameters D. (b) Overall sound pressure level (OASPL) of the single and dual impinging jets at the inner microphone as a function of height, relative to their free-jet configuration. (c) Comparison of acoustic spectra at the impingement height of $H/D = 4$ demonstrates impinging tone modulation and mode switching from $n = 5$ to 4 in the DIJ configuration (green and red circles represent an increase and decrease in tonal amplitudes, respectively) [4].

mode switching from $n = 5$ to 4, and more generally explain how and why acoustic coupling reinforces particular impinging tones and at which heights.

Supplementary supporting evidence of acoustic coupling may be inferred from the SIJ stability analyses of Karami *et al.* [7,29], who examined shear-layer receptivity to determine the optimal frequency and wavelengths internalized by a small pressure perturbation. The study was performed as an angular sweep of acoustic pulse locations with respect to the nozzle center axis. The results have direct implications for DIJ acoustic coupling, since they suggest that maximum shear-layer instability gain may occur on inboard locations of the shear layers, which are susceptible to acoustic disturbances incident between 15° and 45°. The DIJ system clearly contains such acoustic pulse trajectories toward the inboard nozzle region that are sourced from the opposite jet impingement. Valuable insights on acoustic coupling are also obtained from free multijet experiments with the analogous situation of the screech feedback mechanism, which also occurs in the shock-containing supersonic jets studied here. Global modal behavior and discrete tone/mode staging have likewise demonstrated modulation of single jet screech tone predictions in twin configurations [12,30]; these modes have recently been characterized through high-resolution schlieren correlation techniques by Knast *et al.* [31] and linear stability analysis by Nogueira and Edgington-Mitchell [28]. Raman *et al.* addressed these coupling effects by modeling the interjet feedback path of acoustic disturbances as a function of nozzle separation distance to understand global resonance across two screeching free jets [32] and an array of many jets [30]. This methodology has influenced the proposed DIJ coupling model in this current work.

In mixed DIJ (MDIJ), the nozzle exit conditions of the two jets are different, and the fountain flow is biased towards the weaker jet, modulating its SIJ dynamics more so than that of the stronger jet [19]. In this case, hydrodynamic coupling from direct fountain-flow interactions with the shear layer influences the downstream component of the feedback loop, inducing azimuthal variation of impingement characteristics, and thus the acoustics [24,33]. Hromisin *et al.* [34] analyzed MDIJ through a series of experiments by correlating pressure fluctuations at the plate to the near-field acoustics, and relating the propagation paths and signal delays across a range of impingement heights. The computational studies of Stahl and Gaitonde [24,35] examined a Mach 1 and 1.5 MDIJ configuration to find a significant increase in hydrodynamic fountain-flow coupling affecting the shear-layer dynamics. Several MDIJ acoustic experiments by Bhargav *et al.* [36] characterized the effects of momentum and temperature ratios, fully displaying the consequences of the fountain-flow coupling on the acoustic spectra. Since our focus is on acoustic coupling, and hydrodynamic effects can dominate MDIJ, we exclude such systems from the present investigation; however, the proposed DIJ feedback model framework is introduced in general terms to account for mixed jets, and considerations pertinent to such systems are also discussed.

In summary, the goal of this work is to develop a model for DIJ acoustics with the following components: (i) extend the framework of Powell's SIJ feedback model to account for coupled acoustic feedback from a second jet, (ii) introduce a "coresonance" metric that predicts the augmentation of SIJ impinging modes due to this additional coupled feedback loop, and (iii) validate the new theoretical model with experimental acoustic measurements and computational evidence for identical impinging jets. Section II proposes the extended DIJ feedback model, which assimilates the two nominal SIJ feedback loops with the deduced third, globally coupled DIJ feedback loop. The coresonance factor that couples the three loops is also introduced. Experimental DIJ acoustic characteristics of identical Mach 1.27 underexpanded impinging jets over a range of impinging heights [4] are introduced in Sec. III. The model is calibrated using a case study at $H/D = 4$ featuring a large eddy simulation [26] validated by comparison with experimental data; in addition to providing model inputs, the analysis also provides insights into the coupling mechanisms. In Sec. IV, the validity of the model is demonstrated by comparing its predictions with experimental acoustic measurements for a range of heights. Considerations of the model features and some comments on future generalization to MDIJs are also put forth in Sec. IV, and conclusions are presented in Sec. V.

II. DUAL IMPINGING JET FEEDBACK MODEL

A. DIJ acoustic feedback loops and equations

Figure 3 illustrates the different feedback paths in a DIJ system using two jets denoted A and B. The SIJ feedback loop [Fig. 3(a)] is illustrated with paths $1-2$ for jet A and $3-4$ for B in the outboard region of each jet; these loops are relatively isolated from interactions with the other jet. Figure 3(b) sketches the acoustic wavefront produced by the inboard impingement of jet A, which follows both a self-reinforcing SIJ feedback path 2a and simultaneously the coupling path 2b, which crosses through the middle fountain-flow region towards the opposite jet nozzle. Path 2b effectively couples the DIJ system when it is received at the nozzle exit of jet B, which is later than when path 2a affects the nozzle of jet A. Reciprocally, Fig. 3(c) depicts the reversed one-way coupling from inboard impingement events in jet B that constitutes self-reinforcing SIJ feedback path 4a and coupled feedback path 4b.

The one-way acoustic coupling mechanisms introduced in Figs. 3(b) and 3(c) induce shear-layer instabilities through the receptivity process at each nozzle exit. Together, all inboard paths effectively close a two-way coupled feedback loop. Figure 3(d) illustrates the DIJ feedback loop (yellow) that coexists with the SIJ feedback cycles in each jet (red and blue) through shared inboard shear-layer convection and impingement sound production. In this "coupled DIJ feedback" mechanism, a perturbation at the nozzle-exit of A follows the circuit 1-2b-3-4b-1 in Figs. 3(a)–3(c). When this mechanism is superposed on and resonates with the individual SIJ loops, coupled resonance or coresonance is obtained, with implication on the near and far acoustic fields.

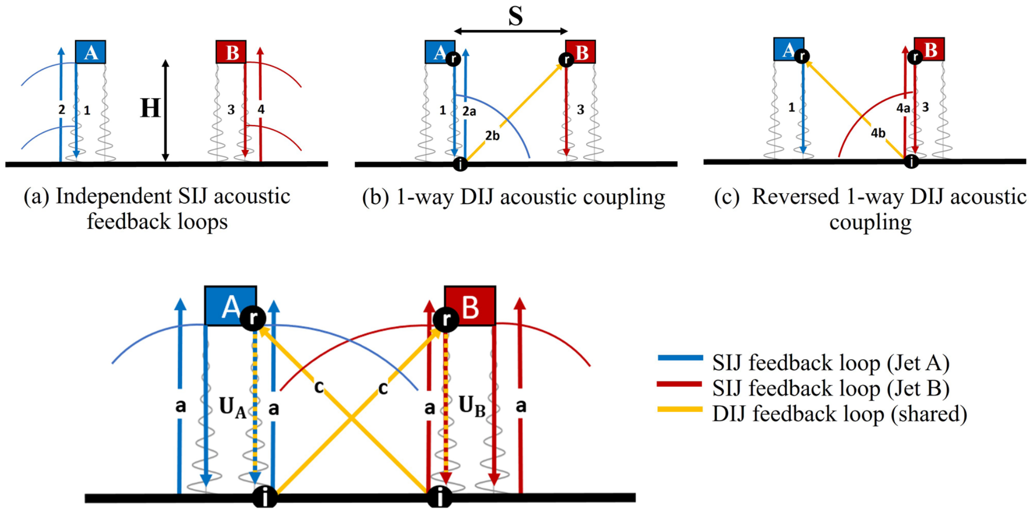

(a) Independent SIJ acoustic feedback loops (b) 1-way DIJ acoustic coupling (c) Reversed 1-way DIJ acoustic coupling

(d) Three coupled feedback loops

FIG. 3. Acoustic feedback mechanisms for a DIJ system. (a) The fundamental SIJ acoustic feedback in each jet illustrated on outboard sides with downstream (paths 1,3) and upstream (paths 2,4) components. (b) The one-way acoustic coupling from jet A to jet B (path 2b) and concurrent self-reinforcing feedback path (path 2a) on the inboard sides. (c) Reciprocal one-way coupling paths from jet B to A. (d) Superposition of all acoustically coupled, closed-loop, DIJ feedback paths, including those associated with each SIJ. Shared receptivity and impingement points are denoted r and i, respectively. Downstream convection speeds are marked U_A and U_B, while acoustic speeds are denoted as a for self feedback and c for coupled feedback. Individual values for each signal are derived in the text.

Equations analogous to those of Powell's SIJ feedback model [2] may be introduced to relate cycle frequencies with the timescales of each of the three individual signal loops. The associated speed of each signal path is marked in Fig. 3(d). The SIJ acoustic feedback signals propagate at the ambient speed of sound a on the inboard and outboard sides; this is a good assumption for the cold identical jets under consideration [26]. The acoustic coupling speed between the two jets is differentiated as c. Although nominally equal to the ambient speed of sound a, this distinction leaves open the possible generalization for hot jets, where the fountain-flow region may display a different acoustic coupling speed. The shear-layer convection speeds, U_A and U_B, depend on individual jet operating conditions and impingement height [17,37,38], but they are equal for IDIJ.

The first step is to invoke Powell's approach for SIJs and consider each jet as if it were isolated; this provides the fundamental impinging feedback frequencies F_A and F_B.

$$\frac{1}{F_A} = \frac{H}{U_A} + \frac{H}{a}, \qquad \frac{1}{F_B} = \frac{H}{U_B} + \frac{H}{a}. \tag{2}$$

To aid in describing the model, the integer mode number n of Eq. (1) is set to unity for now; Sec. II B generalizes the results to arbitrary n. The phase lag p [see Eq. (1)] could be added, however the situation is more complicated since phase lags are required for each jet and the interjet coupling process. For simplicity, the phase-lag is folded into the hydrodynamic term, which assumes an effective average shear-layer convection speed for each jet, U. Measurements in Sec. III incorporate this assumption by finding the effective speed that produces the observed impinging tones. Empirical models, such as those used by Gojon *et al.* [17,39], then calculate convection speed as a function of impinging height.

The time required for signals to propagate along different components of each loop may be added in a straightforward fashion as the ratio of the path length traveled to the speed of signal propagation.

Thus, the time for a signal to propagate from the receptivity location of jet A to that of B, i.e., path 1-2b, is designated $1/G_{AB}$:

$$\frac{1}{G_{AB}} = \frac{H}{U_A} + \frac{\sqrt{H^2 + S^2}}{c}. \tag{3}$$

Adding the resulting shear-layer instability in jet B, i.e., the time associated with path 1-2b-3, is

$$\frac{1}{J_{AB}} = \frac{H}{U_A} + \frac{\sqrt{H^2 + S^2}}{c} + \frac{H}{U_B}. \tag{4}$$

Note that for clarity, G and J are used to designate paths that end in receptivity or impingement points, respectively. Similarly, the time for a signal to propagate on the reciprocal path, 3-4b-1, is

$$\frac{1}{J_{BA}} = \frac{H}{U_B} + \frac{\sqrt{H^2 + S^2}}{c} + \frac{H}{U_A}. \tag{5}$$

Therefore, in any DIJ system, there is a common, acoustically coupled time period, $1/J_{\text{DIJ}}$ that connects events at the nozzle receptivity region of one jet to the delayed impingement of the other jet:

$$J_{\text{DIJ}} = J_{AB} = J_{BA}. \tag{6}$$

The time associated with the complete DIJ two-way acoustically coupled feedback loop, 1-2b-3-4b (or reciprocally 3-4b-1-2b), $1/G_{\text{DIJ}}$ is thus

$$\frac{1}{G_{\text{DIJ}}} = \frac{H}{U_A} + \frac{2\sqrt{H^2 + S^2}}{c} + \frac{H}{U_B}. \tag{7}$$

While the geometric derivations of G_{DIJ} and J_{DIJ} are straightforward, they are not well suited for *a priori* calculation of tones in the acoustic spectra, as these values are at much lower frequencies and encompass multiple impingement events. Rather, the coupled acoustic feedback loop G_{DIJ} is posed as the underlying dynamic that *augments* the SIJ acoustic feedback resonance, which continues to be crucial for the tonal behavior of each jet [4]. For instance, G_{DIJ} and J_{DIJ} are associated with SIJ feedback paths, F_A and F_B; as such, these mechanisms can be related to each other but require the consideration of mode number n, which is added to the model next. G_{DIJ} is primarily responsible for global resonance because of the closed loop nature of its constituent paths; J_{DIJ} does not represent a closed loop, therefore it is not a relevant frequency for this purpose.

B. Coresonance model

The coupling between the jets is now discussed in terms of coresonance, which requires correlation between the different feedback loops and consideration of impinging mode number (n), phases, and signal speeds. The three fundamental feedback equations [Eq. (2) for each jet A and B, and Eq. (7)], which determine F_A, F_B, and G_{DIJ}, enable conditions for global resonance resulting from synchronization of the individual SIJ and the coupled DIJ feedback loop. We introduce a "coresonance" factor to identify this condition, which considers the individual SIJ feedback effects as being compounded by the repeated forcing through the underlying coupled DIJ feedback. This approach is similar to the modulation of Rossiter feedback tones in shallow double cavity flows due to a coupling interaction with lower frequency modes [40,41]. Coresonance is anticipated if the speeds and phases of the SIJ and DIJ feedback sequences align; one manifestation would be if impingement acoustic waves from both jets are simultaneously received at a given nozzle-exit to force the shear-layer instability at regular intervals.

To illustrate this sequence, consider the nozzle receptivity region of jet A. The time delay P_A between the arrival of the SIJ acoustic feedback (path 2a in Fig. 3) and the two-way DIJ feedback signal (path 4b) may be written as

$$P_A = \frac{1}{G_{\mathrm{DIJ}}} - \frac{1}{F_A} = \frac{2\sqrt{H^2+S^2}}{c} + \frac{H}{U_B} - \frac{H}{a}. \tag{8}$$

The corresponding expression for jet B, P_B is

$$P_B = \frac{1}{G_{\mathrm{DIJ}}} - \frac{1}{F_B} = \frac{2\sqrt{H^2+S^2}}{c} + \frac{H}{U_A} - \frac{H}{a}. \tag{9}$$

If the delay time P is zero, then the acoustic waves of the fundamental SIJ and DIJ cycles are synchronized to arrive at the same time. Of course, the path for the DIJ loop is much longer than that for SIJ, so integer multiples become necessary, as incorporated with SIJ mode number n based on the following considerations.

Instead of assessing the time delays P_A and P_B, an alternative approach to characterize the synchronization of the three feedback loops is based on the relative magnitudes of feedback timescales, such as the nonlinear delayed saturation model formulated by Villermaux *et al.* [42] for an array of free jets. More recently, the single jet screech feedback analysis of Mercier *et al.* [37] obtained the optimal resonance mode by observing the delay of acoustic feedback arrival times at the nozzle from sound generated at multiple shock cell locations in the jet. The results indicate that the dominant screech mode is dependent on the number of shorter screech cycle periods of each sound source occurring within the longer feedback loop, which was always an integer value. This perspective is similar to the investigation of the self- and cross-excitation screech feedback of twin free jets by Jeun *et al.* [43]. They note that eligible *points of return* that yield constructive phase criteria with the nozzle receptivity location may be calculated from the requirement that the ratio of cross-correlation time delays to the total screech period be an integer. Influenced by these perspectives of phase delay on multifeedback systems, the DIJ system here is postulated to resonate at integer superharmonics (overtones) of the SIJ feedback frequencies F and the coupled DIJ feedback frequency G_{DIJ}.

This approach is facilitated by first considering real number ratios, N_A and N_B for jets A and B, respectively, representing ratios of the higher SIJ to lower DIJ fundamental frequencies,

$$N_A = F_A/G_{\mathrm{DIJ}}, \quad N_B = F_B/G_{\mathrm{DIJ}}. \tag{10}$$

Substituting Eqs. (2) and (7), we obtain

$$N_A = \frac{a(HcU_B + U_AU_B\sqrt{S^2+H^2} + U_AHc)}{HcU_B(a+U_A)}, \tag{11}$$

$$N_B = \frac{a(HcU_2 + U_AU_B\sqrt{S^2+H^2} + U_AHc)}{HcU_A(a+U_B)}. \tag{12}$$

We now reintroduce SIJ mode number n into the analysis. The dominant SIJ impinging tones of each jet already occur at their preferred mode number. Therefore, it is logical to include n in the determination of N through the expressions

$$N_A = \frac{n_AF_A}{G_{\mathrm{DIJ}}}, \quad N_B = \frac{n_BF_B}{G_{\mathrm{DIJ}}}, \quad n = 1, 2, 3 \ldots . \tag{13}$$

Based on the approaches of the previously discussed multifeedback systems, coresonance occurs when N is an integer value. Depending on the geometric parameters (S, H) and signal speeds, the coupled DIJ feedback signal will arrive at the same time as the SIJ feedback signal when this condition is met. In general, unique values for N_A and N_B are considered such that SIJ resonance with the global frequency G_{DIJ} may occur for neither, one, or both jets, theoretically extending the model to any mixed DIJ conditions. A special case arises if *both* SIJ feedback loops are synchronized to the DIJ feedback loop with integer values of N. Then the jets are "coresonant" with compounded feedback instabilities, resulting in louder acoustic tones in the far field for impinging mode n. For IDIJ, $N_A = N_B = N$, and both jets will have the same resonance characteristics.

To better quantify the near coresonant conditions between SIJ and DIJ cycle alignment, individual resonance factors R_A and R_B are defined for each jet ratio N_A and N_B relative to their nearest integer values

$$R_A = |N_A - \text{round}(N_A)|, \qquad R_B = |N_B - \text{round}(N_B)|, \tag{14}$$

where "round( )" refers to the closest whole number. Differences between the real values N and their nearest integer values produce an individual jet resonance factor ranging from 0 to 0.5. When $R_A = 0$, N_A is an integer, and conditions for SIJ and DIJ feedback loops to synchronize are met. On the other hand, if $R_A = 0.5$, the SIJ and DIJ cycles are dissonant and coupled resonance is not indicated. Furthermore, a relative measure of coresonance, when all three feedback cycles are synchronized, can be defined by the coresonance factor, R_{DIJ}, on a scale from 0 to 1 by accounting for individual resonance factors from each jet:

$$R_{\text{DIJ}} = 1 - (R_A + R_B). \tag{15}$$

Using this metric, global coresonance is defined for a particular SIJ feedback mode n if $R_{\text{DIJ}} = 1$. This global coresonant state is similar to the synchronization and coupling of complex multifaceted feedback flows [32,41,42,44] that demonstrate peak spectral resonance at harmonics when specific geometric conditions facilitate the merging of the periodic dynamics of the two components. The comparable coresonant condition proposed here seeks to explain nonlinear, semidiscrete changes in acoustic power generated from each feedback mode n, with the secondary goal of replicating the OASPL trends. This uncovers circumstances in which global modes in the underlying dynamics become important for specific SIJ impinging tones [4,19,34,45].

In the next section, phenomenological evidence of the proposed DIJ feedback model is presented with experimental data and numerical simulations. The acoustic characteristics of the DIJ system studied there are then directly compared with the model prediction of coresonance factors R_{DIJ} in Sec. IV.

III. EXPERIMENTAL AND SIMULATED NEAR-FIELD ACOUSTICS

A. Impinging jet system

The DIJ acoustic feedback model is tested on two identical, cold Mach 1.27 underexpanded (nozzle pressure ratio 2.65) impinging jets, separated from each other by a distance $S/D = 3.3$ (see Fig. 1 for geometry notation). Experimental measurements are examined over impinging heights $H/D = 3-10$. The experiments use axisymmetric converging nozzles with an exit diameter of $D =$ 25.4 mm and a lip thickness of 0.015 D. Complete details of the experimental setup can be found in [4]. A high-fidelity large-eddy simulation (LES) is used to examine the near-field acoustic feedback paths and calibrate the model at $H/D = 4$ where significant SIJ-DIJ impinging tone modulation is observed. Details of the numerical methods and validation are provided in [24,26]. For reference, instantaneous snapshots of this case study are shown in Fig. 4 with (a) an experimental shadowgraph image and (b) the corresponding LES flow field. The nozzles in the LES are modeled as a constant area sleeve with a sonic outflow condition expanded to Mach 1.27. A nozzle thickness of 0.005 D is used, which is considered thin [46], however other SIJ cases not shown here tested larger nozzle thicknesses and found no change in acoustic tones.

B. SIJ and DIJ acoustic tones

Extensive experimental and numerical data on the acoustics of impinging jets [3,4,21,26,36] indicate strong dependence on H/D. A summary is now presented for reference. The inner microphone [see Fig. 2(a)] positioned equidistant between the jet axes and out of plane at a radial distance of 15 D best captures the interior feedback mechanisms. In contrast, the outer positioned microphone

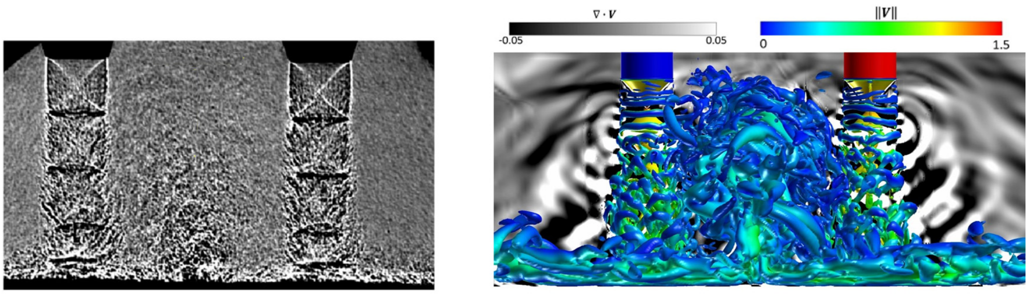

(a) (b)

FIG. 4. Instantaneous snapshot of identical Mach 1.27, underexpanded (NPR = 2.65), cold, round jets showing (a) experimental shadowgraph, and (b) large eddy simulation depicting vorticity isosurfaces and the dilatation field. The coresonance model is calibrated to this case where $S/D = 3.3$ and $H/D = 4$.

primarily isolates SIJ dynamics [4]; these will be introduced later to assess directionality of the sound-field. Dominant SIJ and DIJ acoustic tones from the inner microphone acoustic spectra are characterized in Fig. 5 as a function of height H/D, where frequency is nondimensionalized as $\mathrm{St} = fD/U_j$ and U_j is the jet exit velocity. Phase-averaged shadowgraph analysis [4] indicates that in addition to screech tones, amplitude dominant (loudest) and weaker impinging tones may be distinguished in their axisymmetric and nonaxisymmetric manifestations. Each of these is marked in Fig. 5. Impinging tones are mapped onto the predicted results of Powell's SIJ feedback formula [blue curves, Eq. (1)] to determine which mode number n they belong too. As anticipated, even in the DIJ case, the peak tones generally fall on the SIJ feedback tone curves, indicating continued resonance in the DIJ configuration as well. Impinging tones occur near $\mathrm{St} = 0.35$ and 0.55 and display discrete jumps in frequency as the height is varied, indicative of "staging behavior" between modes [47].

The key takeaway from Fig. 5 is that the influence of the second jet dampens the amplitude dominant axisymmetric tones in the SIJ (black circles) and prefers the lower-frequency nonaxisymmetric impinging tones. Impinging tones related to the $n = 4$ and 5 modes undergo the mode switching in

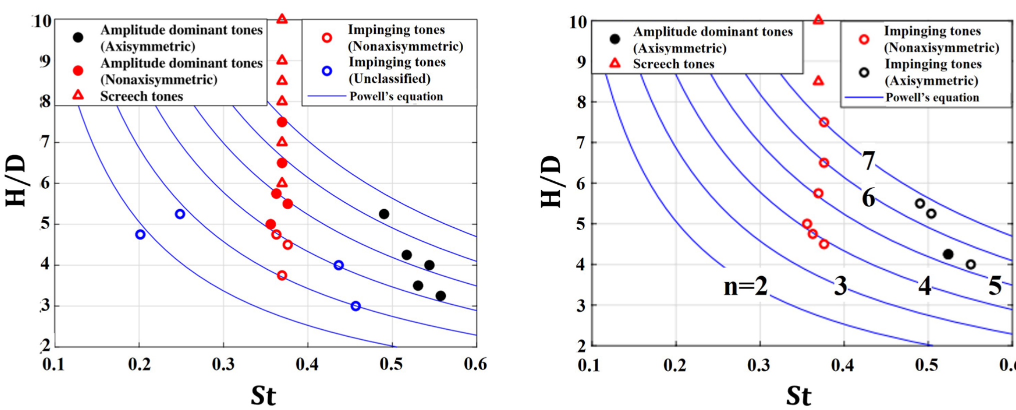

(a) SIJ (b) DIJ

FIG. 5. Peak acoustic tones from spectra taken at the "inner" microphone location are compared to frequencies obtained from Powell's feedback formula for (a) SIJ and (b) DIJ configurations. Mode switching behavior is observed as a function of height with further modulation under DIJ conditions.

the SIJ as a function of height, and more pertinently, further modulation in the DIJ configuration. This phenomenon is strongest near $4 < H/D < 5$ and will be examined more closely using acoustic spectra in Sec. IV when comparing with the co-resonance model. To achieve this, model inputs are first taken from the LES near-field acoustics at $H/D = 4$, where the SIJ impinging tones are loudest.

C. Near-field feedback path illustration

Evidence of the modeled near-field acoustic feedback paths introduced in Sec. II is presented for the case study at $H/D = 4$. An elegant manner to distinguish between the acoustic and hydrodynamic fields is to use momentum potential theory (MPT) [48,49] on the near-field LES solution. A prior application of MPT for the DIJ problem may be found in Stahl *et al.* [21]. MPT splits the "momentum-density" vector, $\rho\vec{u}$; however, it is convenient to extract the dynamics from the primary axial scalar hydrodynamic (B_X) and acoustic ($\partial\psi'_A/\partial X$) components. A sequence of snapshots from this decomposition is shown in Fig. 6 with the corresponding paths from Fig. 3 also displayed on the right side of each frame. The figure reveals the downstream coherent structures within the columns of the jets as well as the acoustic waves propagating outside. At time t_1, the large-scale hydrodynamic structures in the shear layer are highlighted by arrows; these constitute elements of the downstream paths 1 and 3 in Fig. 3 that convect with speed U. The acoustic field of the inboard region displays constructive and destructive interference of multiple passing acoustic waves from impinging jets, shock-associated noise, and turbulent sources. Repeated propagating wavefront patterns are evident, however, which are very pertinent to the acoustic coupling between the jets; a few representative wavefronts are marked in Fig. 6 with dashed curves.

The instant t_2 in Fig. 6 is indicative of the genesis of an acoustic wave after the impingement of an antecedent coherent structure on the inboard side of the left jet (black circle). The solid arrows identify the propagation path (marked 2a and 2b) of the subsequent acoustic wave. Part of an earlier wavefront of the same family is clearly observed as it interacts with the right jet at the nozzle exit (yellow dashed curve). This essentially couples the jets (path 2b), due to the receptivity process and associated downstream convection path 3. Corresponding details of the analogous SIJ process have been discussed by Karami *et al.* [7,29] in the context of hydrodynamic shear-layer instabilities caused by similarly directed acoustic forcing paths. Note that this coupling mechanism coexists with the self-reinforcing feedback path for the same acoustic wave; for example, path components 2a and 2b both trigger shear-layer instabilities in each jet.

In contrast to the complex interior acoustic coupling, snapshot t_3 illustrates an instant which highlights isolated SIJ acoustic feedback on the outboard sides of the jets (paths 2 and 4). The side-to-side differences in phase and acoustic wavelengths are predominately related to the asymmetric jet modes observed in experiments [3,4] and simulated modal analysis [26]; however anomalous intermittent behavior is also observed. Occasionally, impingement events in both jets are simultaneous, resulting in strong acoustic waves that propagate in-phase across the entire DIJ system as shown at time instance t_4. This intermittent strengthening of acoustics across both jets is deduced below to coincide with synchronization of the SIJ and DIJ feedback loops and the coresonance condition.

D. Model signal propagation speeds

The observed near-field feedback paths are now quantified to obtain model inputs, which include the jet convection speeds U_A and U_B, speeds of sound a and c, and configuration dimensions S and H. For the IDIJ of interest, the convection speeds are the same; however, the acoustic coupling signal speed c in general may not equal a due to hydrodynamic and thermal effects in the fountain-flow, particularly in the case of hot jets. Various techniques are available to obtain the convection speed [13,17,31,50]. For example, experimental shadowgraph results [4] estimate the downstream convection speed to be $0.6U_j$, where U_j is the fully expanded jet velocity. Likewise, a may be obtained from experimental observations as 343 m/s. However, c cannot be readily obtained from

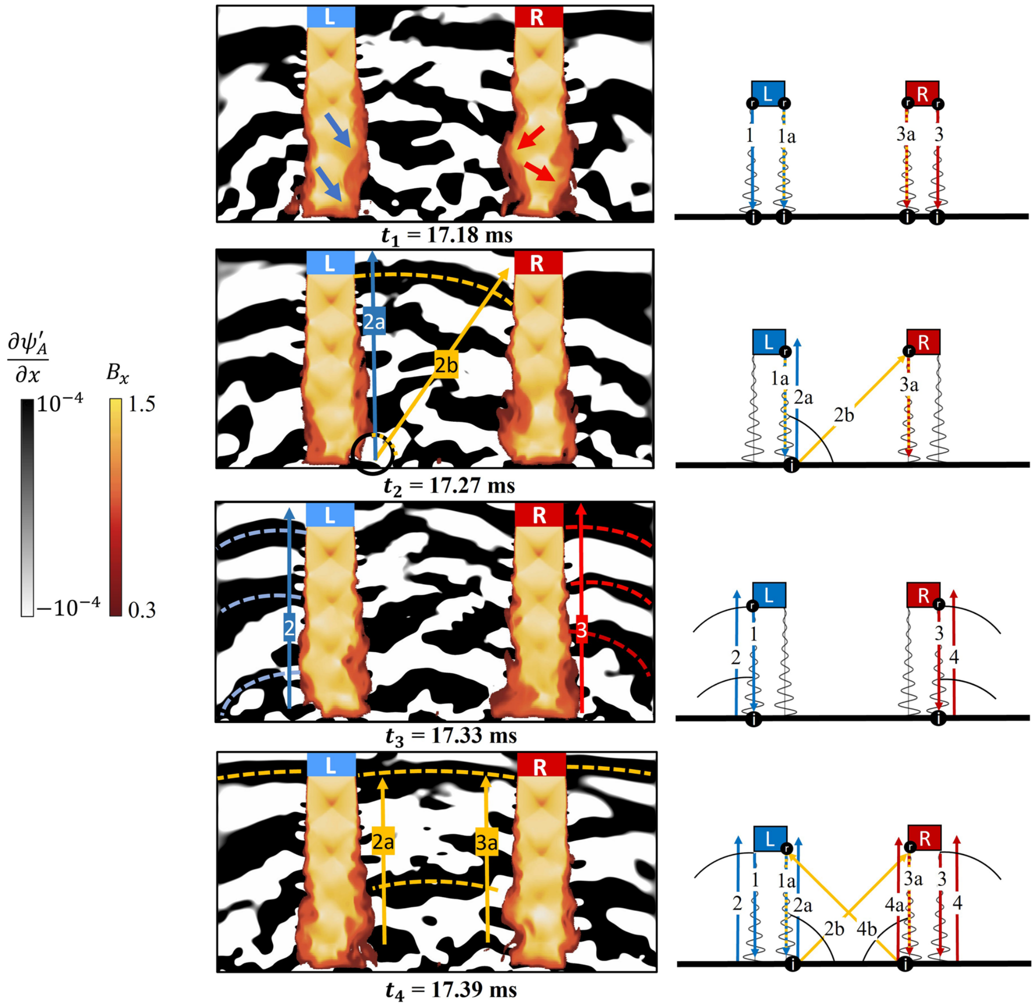

FIG. 6. Hydrodynamic B_X and acoustic $\partial\psi'_A/\partial X$ momentum fields demonstrate the various feedback components over a short time sequence. Contributions to DIJ resonance include large-scale hydrodynamic instabilities (t_1), one-way acoustic coupling (t_2), isolated SIJ feedback behavior (t_3), and synchronized feedback behavior (t_4).

the experimental data, since the turbulent fountain-flow region obscures the coupling acoustic waves (Fig. 4). The MPT decomposed acoustic field is ideally suited for this purpose, since it isolates the propagative component from the hydrodynamic component. For this reason, the LES is used to obtain all input model parameters and compared to experimental measurements and resulting frequencies when available.

The propagation times of the upstream and downstream components of the fundamental SIJ feedback loop (H/a and H/U) and acoustically coupled path ($\sqrt{H^2 + S^2}/c$) are quantified through a cross-correlation analysis of the decomposed acoustic field in Fig. 7. A reference point adjacent to each nozzle exit, Fig. 7(a) is correlated with values along a line of probes in the shear-layer and across the fountain-flow region. The correlation coefficients of each point along the paths are then plotted as functions of lead/lag time delay (τ), normalized by the autocorrelations of each point at zero lag. The peaks and troughs of the correlation function are then associated with propagating

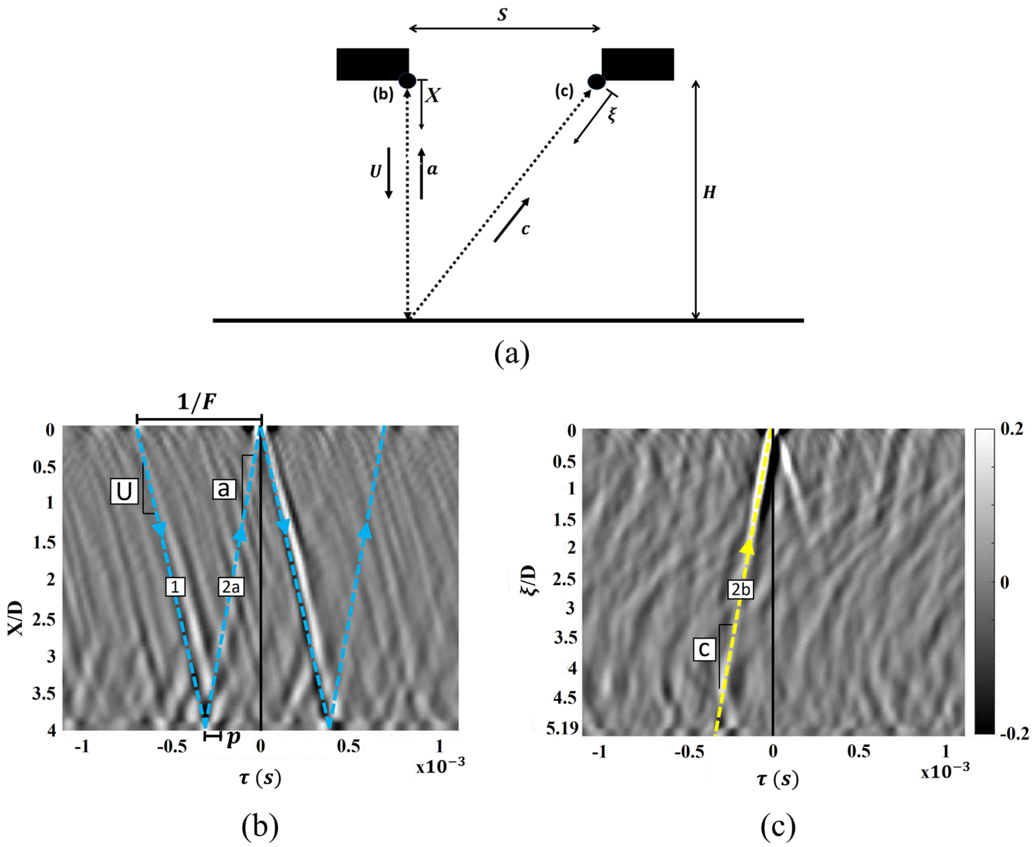

FIG. 7. Normalized cross-correlation of the acoustic momentum field $\partial \psi'_A/\partial X$, taken along two lines of probes with respect to the self-reinforcing and coupled acoustic receptivity points (a). The vertical line along the shear layer (b) captures the upstream a and downstream U components of the SIJ feedback cycle. The path ξ across the fountain-flow region (c) measures the acoustic signal c that couples the jets.

expansion/compression of acoustic signals, averaged over a 1.1 ms sliding window which is long enough to recover at least two full SIJ feedback cycles in each plot.

Figure 7(b) shows correlation results for the inboard self-reinforcing SIJ feedback loop. The peak correlation occurs at the nozzle receptivity point $X/D = 0$, which is also the autocorrelation. The largest peaks at $\tau = 0$ and ± 0.683 ms are interpreted as the rudimentary feedback cycle starting and ending with upstream acoustic receptivity. This corresponds to a frequency of $F = 1{,}462$ Hz. The upstream acoustic process (2a) is traced in blue from the largest coefficient at the plate ($X/D = 4$, $\tau = -0.296$ ms) to the receptivity point $\tau = 0$. The slope of this trace recovers the assumed speed of sound $a = 343.7$ m/s. From this point on the plate, the downstream component (1) may be traced back towards $\tau = -0.683$ ms at the nozzle to obtain the effective downstream shear-layer convection speed, which is calculated as $U = 262$ m/s, confirming the estimate of $0.6U_j$ from experiments. This approach neglects the phase lag p in Eq. (1) associated with the sound production delay, i.e., the averaged effective downstream component is used instead to simplify the DIJ resonance model. The slight deviation between the downstream convection line (1) and the proximal correlation peak (white streak) is associated with this choice. We note that if desired, an estimate for p could be obtained by considering the distance from the local peak-to-trough correlation at the impingement point. This yields an estimated phase lag time of $p \approx 40$ μs, comparable to the study of Weightman [50].

TABLE I. DIJ feedback model inputs for identical DIJ measured at $H/D = 4$. Individual feedback path speeds a, c, and U are used to calculate SIJ feedback tones nF and coupled feedback frequency G_{DIJ}. Highlighted in bold font, the feedback mode $n = 4$ yields the closest value to an integer ratio N based on the underlying coupled feedback frequency G_{DIJ}, and thus the highest coresonance factor R_{DIJ} at $nF = 5850$ Hz.

Model	inputs	SIJ impinging mode (n)	nF (Hz)	G_{DIJ} (Hz)	$N = nF/G_{\mathrm{DIJ}}$	R_{DIJ}
a (m/s)	343.7	1	1463	649	2.26	0.48
c (m/s)	343.7	2	2927		4.51	0.02
U (m/s)	262	3	4390		6.77	0.54
H (m)	0.1016	**4**	**5853**		**9.03**	**0.94**
S (m)	0.0838	5	7316		11.28	0.44

The acoustic coupling signal path, from the impingement of jet A to the receptivity location of jet B, is analyzed in Fig. 7(c). Compared to the clear striation pattern of the SIJ feedback in (b), the acoustic field here is distorted by the underlying turbulent fountain-flow. However, a clear upward signal is observed closer to the nozzle, where the fountain-flow is less influential, and traced (yellow line) back to the peak correlation impingement event. The slope of this line determines the acoustic coupling signal speed. The value obtained matches the nominal speed of sound $c = 343.7$ m/s, i.e., the coupling speed is relatively unaffected by fluctuations from the turbulence. A weak, downward streak in the positive τ direction is also observed, and it is inferred to be the acoustic wave reflected off the nozzle; however, this signal diminishes relatively quickly and has no apparent contribution to the feedback dynamics.

All measured signal speeds and geometric parameters are substituted into the DIJ feedback formulas of Sec. II to determine SIJ impinging tones nF, DIJ feedback frequency G_{DIJ}, ratio N, and coresonance factor R_{DIJ}. Model results are listed in Table I, along with the individual feedback path signal times H/a, $\sqrt{(H^2 + S^2}/c$, and H/U. To examine coresonance over a range of impingement heights, the convection velocity U must also change as a function of H/D [13]. The empirical model of Gojon *et al.* [39] is adapted for this purpose:

$$U(H/D) = 0.65U_j - (0.65U_j - 0.5U_j)\frac{1}{1 + H/D} - 0.017U_j. \tag{16}$$

This formulation is calibrated to match the measured convection speed from the cross-correlation analysis at $H/D =$ 4. The resulting SIJ feedback tones are then validated with the experimental acoustic spectra in the next section.

IV. DIJ MODEL PERFORMANCE

Results from the DIJ feedback model, using inputs from the $H/D = 4$ case study, are now presented to demonstrate the role of R_{DIJ} in estimating the modulation of SIJ-DIJ impinging tones. This is followed by a comparison of model predictions to acoustic trends over a range of impinging heights, and the model framework is finally extended for future adaptation to any general set of two jets at mixed operating conditions.

A. Coresonance impinging tone modulation

The coresonance factor R_{DIJ} is compared with the SIJ and DIJ acoustic spectra at heights chosen to characterize impinging tone modulation due to acoustic coupling. First, the SIJ-DIJ modulation of impinging tones at the inner microphone is instantiated in Fig. 8(a) at $H/D = 4$, which switches from the SIJ peak tone at $n = 5$ (red circle) to $n = 4$ (green circle) in the DIJ spectra. The augmentation of the $n = 4$ mode by 12 dB suggests DIJ coupling effects are optimal at this mode and height. In contrast, Fig. 8(b) shows the DIJ spectra at $H/D = 10$, which is nearly identical to

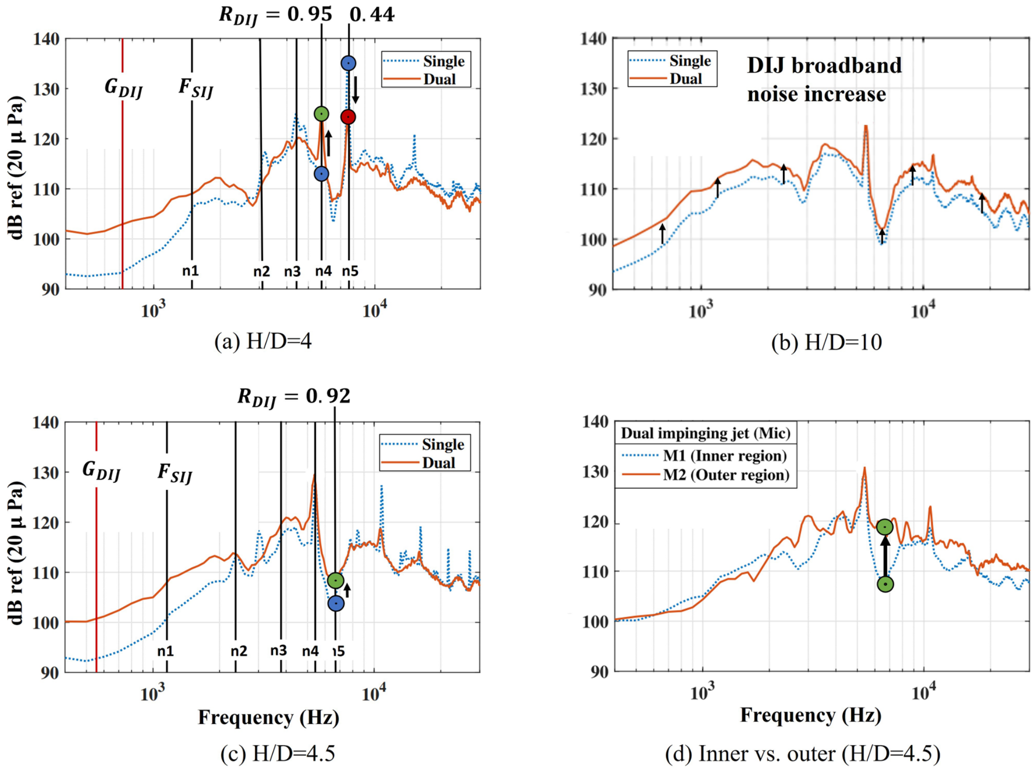

FIG. 8. Experimental acoustic spectra comparing SIJ and DIJ impinging tone characteristics. SIJ feedback tones nF predicted from the model align with peak impinging tones, while the DIJ global frequency G_{DIJ} does not appear. However, its presence manifests in coresonance factors R_{DIJ}, which successfully predicts the increase (green) or decrease (red) of DIJ impinging tones relative to the nominal SIJ spectra (blue). (a) $H/D = 4$ undergoes the most drastic mode switching from SIJ $n = 5$ to DIJ $n = 4$. This coupling behavior is in contrast to the more common broadband DIJ increase, exemplified in (b) at $H/D = 10$. (c) A less prominent coresonance condition also occurs at $H/D = 4.5$ for the $n = 5$ impinging mode. This particular tone is better observed in (d) from the outer microphone location, while all other results are shown for the inner microphone.

the SIJ spectra with a broadband upward 3 dB shift, but no change in the dominant DIJ impinging tone. This comparatively simpler case represents the DIJ broadband increased noise regime, which generally persists for most heights and will be revisited later.

For the present, the change in amplitude of the impinging tones in the DIJ spectra of Fig. 8(a) is explained by the model results listed in Table I. The SIJ impinging tones nF, determined from Powell's formula, are all observed in the acoustic spectra. Focusing on the coupled feedback frequency G_{DIJ}, the 649 Hz frequency is much lower than the prominent SIJ feedback tones and is not explicitly observed in the DIJ spectra of Fig. 8. However, following the framework of the coresonance model, the important parameter is the ratio $N = nF/G_{\text{DIJ}}$. Seeking the integer ratio required for coupled feedback resonance, mode $n = 4$ has the closest value of N to an integer (9.03) with a corresponding coresonance factor $R_{\text{DIJ}} = 0.94$. This may be physically interpreted as requiring approximately nine SIJ feedback signals to occur for every synchronized arrival of the DIJ feedback cycle. Consistent with the spectra of Fig. 8(a), the feedback tone $n = 4$ experiences a significant increase in amplitude from the SIJ case (green circle), supporting the coresonance explanation of G_{DIJ} in augmenting specific impinging tones. Addressing other impinging modes that are out-of-phase with the global feedback loop, such as $n = 2,\ 3$, and 5 ($R_{\text{DIJ}} = 0.02,\ 0.54$, and

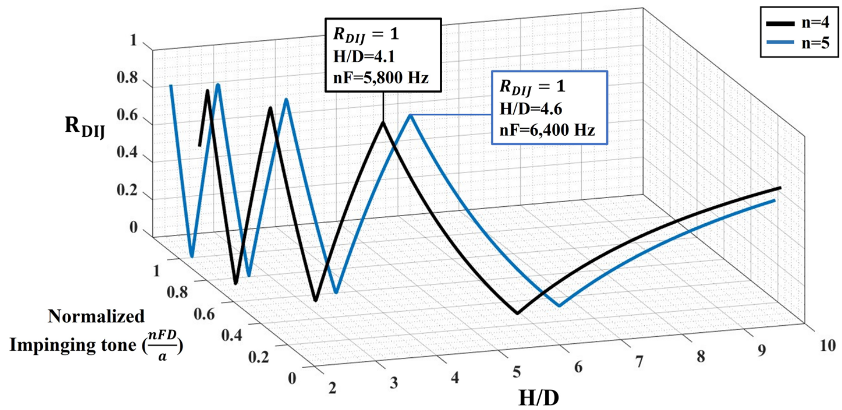

FIG. 9. Coresonance factor R_{DIJ} as a function of normalized impinging tone nFD/a and height H/D. The most prominent impinging modes $n = 4$ and 5 are used to determine the most likely frequencies and heights at which coresonance occurs ($R_{\mathrm{DIJ}} = 1$).

0.44), the model indicates a decrease in each tonal amplitude relative to the baseline SIJ spectra; this is most noticeable in the damping of the loudest SIJ tone $n = 5$ (red circle). However, interpretation of midrange values of R_{DIJ} is ambiguous, therefore significance is only given to extreme in-phase or out-of-phase values of coresonance ($R_{\mathrm{DIJ}} > 0.9$ or $R_{\mathrm{DIJ}} < 0.1$, respectively).

Next consider Fig. 8(c), which is at a height thoroughly dominated by the $n = 4$ mode for both the SIJ and DIJ spectra. Minor amplitude increases in DIJ impinging tones are observed, with only a relatively modest 5 dB change in amplitude for the $n = 5$ mode where $R_{\mathrm{DIJ}} = 0.92$. The predicted coresonance at $n = 5$ is better observed in Fig. 8(d), which compares the DIJ spectra at the outer microphone location. Note that only at this height and mode do the two microphone locations have meaningful differences in the acoustic spectra, possibly due to regions of sound cancellation incurred by particular frequencies and azimuthal symmetries of two jet systems [28,51]. Nevertheless, the relatively subdued modulation at $H/D = 4.5$ does not indicate appreciable coupled resonance for the $n = 5$ mode compared to the loudest $n = 4$ tone. Summarizing Fig. 8, the distinct SIJ and DIJ acoustic characteristics near $H/D = 4$ and 4.5 suggest that the coresonance model can explain anomalous SIJ-DIJ mode switching, but is less meaningful in the height regime that experiences simple DIJ broadband sound increases. This motivates an examination of using R_{DIJ} to effectively predict heights that are susceptible to coresonance.

B. Coresonance over a range of heights

To explore coresonance over a range of heights, consider R_{DIJ} values plotted in Fig. 9 as a function of height (H/D) and SIJ impinging tone frequency, normalized by nozzle diameter and speed of sound (nFD/a). The choice of which modes n to examine is guided by the persistence of amplitude dominant $n = 4$ and 5 tones observed at all heights in both SIJ and DIJ spectra. At heights above $H/D > S/D > 3.3$, where fountain flow effects are limited, the curve shows single peak values of R_{DIJ} at $H/D = 4.1$ and 4.6 for the $n = 4$ and 5 modes, respectively. Not only are these peak coresonance factors in excellent agreement with the 5800 and 6400 Hz impinging tones in the spectra of Fig. 8, but this plot clearly narrows coresonance conditions to only a few possible heights and tones. Examining heights where $R_{\mathrm{DIJ}} = 0$, both modes have out-of-phase DIJ feedback loops near approximately $H/D = 6$. Above this height, the coresonance factor has a gradual rise, but never appreciates to the coresonance condition within the ground effect. This is commensurate with the jet noise profile approaching free-jet levels where screech and broadband noise overtake impingement acoustics [4]. Later, the model will be compared to this height regime to distinguish coresonance from broadband DIJ sound increases.

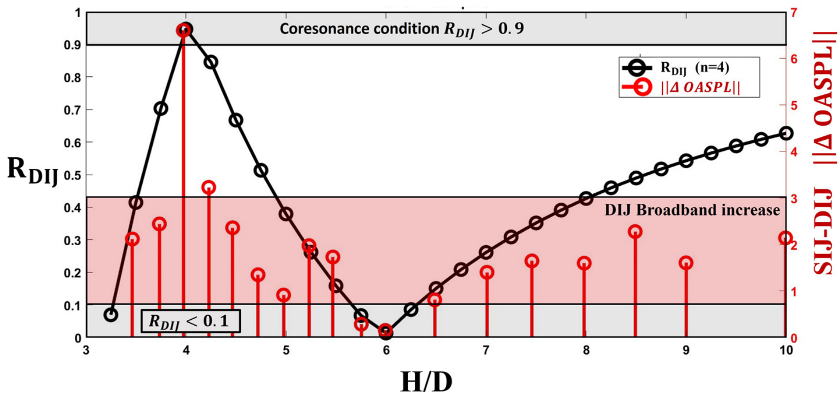

FIG. 10. Coresonance factor R_{DIJ} compared to the SIJ-DIJ OASPL difference as a function of height. The model using the $n = 4$ mode matches the maximum and minimum SIJ-DIJ sound level differences at $H/D = 4$ and 6, respectively. The model also envelopes the regions where broadband DIJ sound increase occurs, banded by a 3 dB range.

Of the two choices in coresonance modes, $n = 4$ is determined to be optimal for acoustic coupling based on peak amplitude observations of Fig. 8. However, the reason for optimality of $n = 4$ over $n = 5$ is not entirely clear. One possibility is that lower frequency asymmetric modes are better suited for coupling. For example, in the SIJ-DIJ mode switch of Fig. 8(a), the SIJ is dominated by the $n = 5$ axisymmetric mode, but the DIJ spectra prefer the lower-frequency $n = 4$ mode, which is asymmetric [4] and found to manifest in the near-field as counter-rotating helical SPOD modes [26]. Bhargav *et al.* also demonstrated that the lower-frequency asymmetric modes persist for both SIJ and DIJ at the majority of heights and in the free-jet configuration [4]; this might be related to the synchronization of the $n = 4$ mode with the screech tone [52,53] that remains consistent across all heights [4]. Other screeching twin free-jet studies have demonstrated a similar preference for coupled, lower-frequency asymmetric modes, shifting away from single-jet axisymmetric modes [31]. Another factor why coupled axisymmetric modes are not preferred could be related to the gain criteria in Powell's feedback formulation [1]. That is, the amplification of acoustic disturbances propagated from the axisymmetric $n = 5$ mode of the opposite jet is not optimal for resonance. These inferences are carried forward in the model by examining only $n = 4$ results over a range of heights.

The coresonance factor R_{DIJ} is now compared to the difference between SIJ and DIJ OASPLs previously introduced in Fig. 2. In addition to comparing model trends, the OASPL difference shown in Fig. 10 delineates between the large region of DIJ broadband noise increase (3 dB range) and unique heights where DIJ coupling significantly modulates noise. As such, the coresonance condition at $H/D = 4$ matches the peak 7 dB OASPL difference and also predicts the out-of-phase coupling at $H/D = 6$ ($R_{\text{DIJ}} < 0.1$) where SIJ-DIJ differences are at a minimum. In between these extremes, the coresonance factor accurately envelopes the SIJ-DIJ OASPL profile, justifying use of the $n = 4$ mode to represent the whole range of heights.

C. Mixed dual impinging jets

Some comments are provided to guide future extension of the theoretical DIJ model framework to any general set of mixed jet operating conditions. As the jets become more disparate, hydrodynamic coupling from the fountain-flow becomes prominent, the effects of which are not modeled in the present work. Nonetheless, important insights can still be obtained regarding acoustic coupling behavior. In these cases, convection velocities U_A and U_B differ, but the same principles of coresonance can be applied, yielding different individual resonance factors in each jet ($R_A \neq R_B$). The

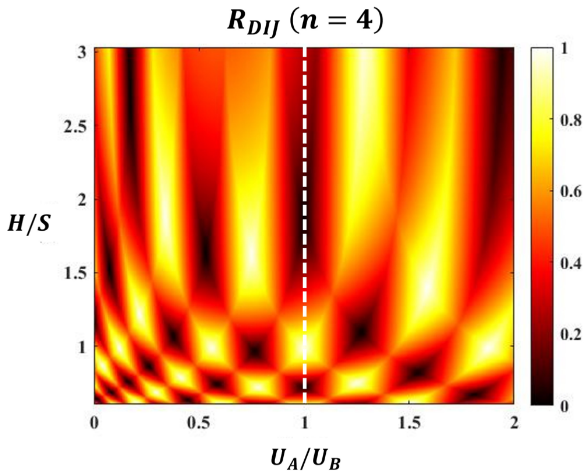

FIG. 11. Coresonance map R_{DIJ} of mixed DIJ jet speeds U_A/U_B and geometric parameters H/S. Model inputs are based on the IDIJ case study represented as the white dashed line.

total coresonance factor R_{DIJ} collapses as a function of the geometric and jet parameters that define the system, H/S and U_A/U_B, respectively, where U_A/U_B is the ratio of shear-layer convection speeds of each jet. Figure 11 shows the resonance map for the entire MDIJ parameter space using the same nominal conditions as the identical jet case study ($n = 4$), represented by the dashed vertical line. The checkered resonance pattern has a reciprocal symmetry about $U_A/U_B = 1$ that displays staging behavior between dissonance and resonance. If $R_{\text{DIJ}} = 1$, then both SIJ feedback loops are perfectly synchronized with the DIJ feedback loop; at these conditions, coresonance and peak noise levels would be expected for that impinging mode. In contrast, Fig. 11 also shows that coresonance is not guaranteed for all mixed jet ratios U_A/U_B, regardless of height. However, extended partial resonance can exist in one jet but not the other, demonstrated by the vertical bands that linger over a range of heights, and confirmed in individual resonance factors R_A or R_B not shown here.

In future development, an expanded coresonance map of this nature may be used for design estimates by choosing aircraft nozzle separation distances and jet operating conditions. For example, the degree of acoustic resonance of a VTOL aircraft during takeoff or descent may be predicted at each height from Fig. 11, and the amplification of specific loading frequencies on the structure or nearby personnel can be determined from Eq. (13). Theoretically, the DIJ acoustic profile could even be predicted from only SIJ experimental data if the jet convection speeds are well calibrated. However, the reality of mixed jet operating conditions is that additional physics must be accounted for in the model, mainly the hydrodynamic coupling of the jets. Other research [21,24,35,36] on MDIJs has demonstrated how the fountain-flow shear-layer interactions modulate the downstream component of the feedback loop, with significant effects as the disparity between U_A and U_B increases. Therefore, the understanding of hydrodynamic coupling remains a crucial link in the adaptation of the DIJ acoustic feedback model for general mixed jet cases. Fortunately, in the absence of strong fountain-flow coupling, the identical DIJ cases can be well characterized by the coresonance feedback model.

V. CONCLUSIONS

A theoretical framework is proposed to model the acoustic feedback coupling of dual impinging jets (DIJs). The DIJ model is an extension of the single impinging jet (SIJ) acoustic feedback model of Powell, and it postulates the existence of a globally coupled DIJ feedback loop that explains observed differences in SIJ-DIJ impinging tone modulation. Three fundamental acoustic feedback loops are introduced: two self-reinforcing SIJ feedback paths that dominate the dynamics of each jet, and a lower frequency coupled DIJ feedback loop that augments the strength of individual SIJ feedback modes with repeated acoustic forcing. The synchronization of all feedback mechanisms poses a “coresonance” condition that is quantified by a coresonance factor on a scale of 0 to 1. The coresonance factor successfully predicts the relative impinging tone amplitude modulation from the nominal SIJ configuration, including SIJ impinging modes most susceptible to reinforced DIJ coupling. In addition, the model matches SIJ-DIJ OASPL trends over a range of heights, and it can distinguish when coresonance emerges from the baseline broadband noise increase due to the addition of the second jet.

The acoustic coupling mechanisms are illustrated using an LES case study of two underexpanded (NPR 2.65) Mach 1.27 jets at an impingement height $H/D = 4$. Momentum potential theory decomposition applied to the LES data isolates the acoustic waves in the turbulent fountain-flow region between the two jets. The resulting instantaneous sequence captures evidence of each acoustic feedback path proposed in the model. A cross-correlation analysis confirms the signal speeds of these feedback paths, which are then used to calibrate the model, and they are validated with acoustic tones observed in the experimental microphone spectra.

Results from the application of the modeled coresonance factor are summarized for a range of impinging heights. The model accuracy at heights further away from the measured input conditions is improved by using an empirical function for the convection velocity. Coresonance detection is recognized for values of $R_{\text{DIJ}} > 0.9$, while the other extreme $R_{\text{DIJ}} < 0.1$ indicates out-of-phase feedback loops, and minimal SIJ-DIJ acoustic differences. Midrange coresonance values can be ambiguous, particularly when examining impinging modes n that do not resonate in the individual jets. Using the optimal SIJ impinging mode, the coresonance comparison supports the theory of an underlying globally coupled feedback loop that synchronizes with the dominant SIJ feedback loops, in a manner that allows for an extension to mixed-jet DIJ configurations. In a generalized sense, the coresonance metric collapses as a function of two ratios in the geometric configuration: the height to separation distance H/S, and the relative jet convection speeds U_A/U_B. However, future models for mixed jets will require further consideration of the hydrodynamic coupling via the fountain-flow, which begins to affect the downstream components of the feedback loops.

ACKNOWLEDGMENTS

This work was funded by the Office of Naval Research under Grant No. N00014-18-1-2506. The opinions, findings, views, conclusions or recommendations contained herein are those of the authors and should not be interpreted as necessarily representing the official policies or endorsements, either expressed or implied, of ONR or the U.S. Government. Computational resources were provided by the DoD High Performance Computing Modernization Program as well as the Ohio Supercomputer Center. Extensive discussions and data from experimental collaborators at Florida Center for Advanced Aero Propulsion, including P. Sellappan and R. Kumar, are gratefully acknowledged.

[1] A. Powell, On edge tones and associated phenomena, Acustica **3**, 233 (1953).

[2] A. Powell, The sound-producing oscillations of round underexpanded jets impinging on normal plates, J. Acoust. Soc. Am. **83**, 515 (1988).

[3] V. N. Bhargav, M. Song, P. Sellappan, F. S. Alvi, and R. Kumar, Unsteady characteristics of resonant supersonic dual impinging jets, in *AIAA Scitech 2020 Forum* (AIAA, Orlando, Florida, 2020).

[4] V. N. Bhargav, M. Song, P. Sellappan, F. S. Alvi, and R. Kumar, Experimental characterization of supersonic single- and dual-impinging jets, AIAA J. **59**, 2282 (2021).

[5] R. Kumar, A. Wiley, L. Venkatakrishnan, and F. Alvi, Role of coherent structures in supersonic impinging jets, Phys. Fluids **25**, 076101 (2013).

[6] S. Karami, D. Edgington-Mitchell, and V. Theofilis, Characteristics of acoustic and hydrodynamic waves in under-expanded supersonic impinging jets, J. Fluid Mech. **905**, A34 (2020).
[7] S. Karami and J. Soria, Influence of nozzle external geometry on wavepackets in under-expanded supersonic impinging jets, J. Fluid Mech. **929**, A20 (2021).
[8] J. C. Carling and B. L. Hunt, The near wall jet of a normally impinging, uniform, axisymmetric, supersonic jet, J. Fluid Mech. **66**, 159 (1974).
[9] J. M. Barata, Ground vortex formation with twin impinging jets, SAE Technical Papers (1996).
[10] C.-M. Ho and N. S. Nosseir, Dynamics of an impinging jet. Part 1. The feedback phenomenon, J. Fluid Mech. **105**, 119 (1981).
[11] N. S. Nosseir and C.-M. Ho, Dynamics of an impinging jet. Part 2. The noise generation, J. Fluid Mech. **116**, 379 (1982).
[12] G. Raman, Advances in understanding supersonic jet screech, Prog. Aerosp. Sci. **34**, 45 (1998).
[13] A. Krothapaili, E. Rajkuperan, F. Alvi, and L. Lourenco, Flow field and noise characteristics of a supersonic impinging jet, in *4th AIAA/CEAS Aeroacoustics Conference, Toulouse, France*, Vol. 392 (AIAA, Reston, VA, 1998), pp. 155–181.
[14] A. Krothapalli, On discrete tones generated by an impinging underexpanded rectangular jet, in *AlAA 8th Aeroacoustics Conference, Atlanta, GA*, Vol. 23 (AIAA, Reston, VA, 1983), p. 1910.
[15] N.-H. Liu, X.-R. Li, P.-F. Hao, X.-W. Zhang, and F. He, Mode switch in tonal under-expanded impinging jets, Phys. Fluids **33**, 124102 (2021).
[16] D. Edgington-Mitchell, Aeroacoustic resonance and self-excitation in screeching and impinging supersonic jets—A review, Int. J. Aeroacoust. **18**, 118 (2019).
[17] C. Bogey and R. Gojon, Feedback loop and upwind-propagating waves in ideally expanded supersonic impinging round jets, J. Fluid Mech. **823**, 562 (2017).
[18] D. Kotansky and L. Glaze, The effects of ground wall-jet characteristics on fountain upwash flow formation and development, in *14th Fluid and Plasma Dynamics Conference, Palo Alto, California* (AIAA, Reston, VA, 1981).
[19] L. M. Myers, N. Rudenko, and D. K. McLaughlin, Investigation of the flow-field of two parallel round jets impinging normal to a flat surface, in *54th AIAA Aerospace Sciences Meeting* (AIAA, Reston, VA, 2016), p. 1.
[20] M. Song, V. N. Bhargav, S. Seckin, P. Sellappan, R. Kumar, and F. S. Alvi, Active flow control of single and dual supersonic impinging jets using microjets, in *AIAA Scitech 2021 Forum* (AIAA, Reston, VA, 2021).
[21] S. L. Stahl and D. Gaitonde, Analysis of fountain-flow coupling between twin sonic impinging jets, in *AIAA Aviation 2021 Forum* (AIAA, Reston, VA, 2021), pp. 1–19.
[22] A. J. Saddington, P. M. Cabrita, and K. Knowles, *Engineering Turbulence Modelling and Experiments 6* (Woodhead Publishing Limited, 2005), pp. 667–676.
[23] A. J. Saddington, K. Knowles, and P. M. Cabrita, On the characteristics of a twin-jet STOVL fountain, Aeronaut. J. **113**, 139 (2009).
[24] S. L. Stahl and D. V. Gaitonde, Computational investigation of dual impinging jet dynamics at mixed operating conditions, in *AIAA Scitech 2020 Forum, Orlando, Florida* (AIAA, Reston, VA, 2020).
[25] M. Wong, Dynamic coupling effects on twin supersonic impinging jets, in *54th AIAA Aerospace Sciences Meeting, San Diego, California* (AIAA, Reston, VA, 2016).
[26] S. L. Stahl, C. Prasad, and D. V. Gaitonde, Distinctions between single and twin impinging jet dynamics, J. Acoust. Soc. Am. **150**, 734 (2021).
[27] Y. Mehta, K. Natarajan, P. Sellappan, J. Gustavsson, and R. Kumar, Effect of nozzle spacing in supersonic twin impinging jets, AIAA J. **60**, 2423 (2021).
[28] P. A. Nogueira and D. M. Edgington-Mitchell, Investigation of supersonic twin-jet coupling using spatial linear stability analysis, J. Fluid Mech. **918**, A38 (2021).
[29] S. Karami, P. C. Stegeman, A. Ooi, and V. Theofilis, Receptivity characteristics of under-expanded supersonic impinging jets, J. Fluid Mech. **889**, A27 (2020).
[30] G. Raman, Coupling of twin supersonic jets of complex geometry, J. Aircraft **36**, 743 (1999).

[31] T. Knast, G. Bell, M. Wong, C. M. Leb, J. Soria, D. R. Honnery, and D. Edgington-Mitchell, Coupling modes of an underexpanded twin axisymmetric jet, AIAA J. **56**, 3524 (2018).
[32] G. Raman and R. Taghavi, Resonant interaction of a linear array of supersonic rectangular jets: An experimental study, J. Fluid Mech. **309**, 93 (1996).
[33] M. L. Houston, J. W. Nichols, F. Zigunov, P. Sellappan, and F. Alvi, Simulations and experiments of dual high-speed impinging jets, in *2018 AIAA/CEAS Aeroacoustics Conference* (AIAA, Reston, VA, 2018).
[34] S. M. Hromisin, L. M. Myers, D. K. McLaughlin, and P. J. Morris, The far-field acoustics of supersonic single and dual impinging jets with correlations to near-field noise, in *AIAA SciTech Forum—55th AIAA Aerospace Sciences Meeting* (AIAA, Reston, VA, 2017), p. 1.
[35] S. Stahl and D. V. Gaitonde, Effects of fountain flow interaction on dual jet impingement at mixed operating conditions, in *AIAA Scitech 2021 Forum* (AIAA, Reston, VA, 2021).
[36] V. N. Bhargav, Y. Mehta, R. Kumar, and F. S. Alvi, Effect of relative momentum and temperature on the aeroacoustic characteristics of dual impinging jets, in *AIAA Aviation 2021 Forum* (AIAA, Reston, VA, 2021), p. 1.
[37] B. Mercier, T. Castelain, and C. Bailly, Experimental characterisation of the screech feedback loop in underexpanded round jets, J. Fluid Mech. **824**, 202 (2017).
[38] P. Pineau and C. Bogey, Temperature effects on convection speed and steepened waves of temporally developing supersonic jets, AIAA J. **58**, 1227 (2020).
[39] R. Gojon, C. Bogey, and O. Marsden, Large-eddy simulation of underexpanded round jets impinging on a flat plate 4 to 9 radii downstream from the nozzle, in *21st AIAA/CEAS Aeroacoustics Conference* (AIAA, Reston, VA, 2016), p. 1.
[40] N. Delprat, Rossiter's formula: A simple spectral model for a complex amplitude modulation process? Phys. Fluids **18**, 071703 (2006).
[41] F. Tuerke, L. Pastur, Y. Fraigneau, D. Sciamarella, and F. Lusseyran, Nonlinear dynamics and hydrodynamic feedback in two-dimensional double cavity flow, J. Fluid Mech. **813**, 1 (2017).
[42] E. Villermaux and E. Hopfinger, Self-sustained oscillations of a confined jet: A case study for the non-linear delayed saturation model, Physica D **72**, 230 (1994).
[43] J. Jeun, G. J. Wu, and S. K. Lele, Aeroacoustic coupling in twin supersonic rectangular jets, in *AIAA Aviation 2021 Forum* (AIAA, Reston, VA, 2021).
[44] F. Tuerke, L. R. Pastur, D. Sciamarella, F. Lusseyran, and G. Artana, Experimental study of double-cavity flow, Exp. Fluids **58**, 76 (2017).
[45] M. Harmon, V. N. Bhargav, P. Sellappan, F. S. Alvi, and R. Kumar, Experimental study of impinging jet flow field involving converging and CD nozzle pair, in *AIAA Aerospace Sciences Meeting, Kissimmee, Florida* (AIAA, Reston, VA, 2018), p. 1.
[46] J. L. Weightman, O. Amili, D. Honnery, D. Edgington-Mitchell, and J. Soria, Nozzle external geometry as a boundary condition for the azimuthal mode selection in an impinging underexpanded jet, J. Fluid Mech. **862**, 421 (2019).
[47] S. I. Kim and S. O. Park, Oscillatory behavior of supersonic impinging jet flows, Shock Waves **14**, 259 (2005).
[48] P. E. Doak, Momentum potential theory of energy flux carried by momentum fluctuations, J. Sound Vib. **131**, 67 (1989).
[49] S. Unnikrishnan and D. V. Gaitonde, Acoustic, hydrodynamic and thermal modes in a supersonic cold jet, J. Fluid Mech. **800**, 387 (2016).
[50] J. L. Weightman, O. Amili, D. Honnery, J. Soria, and D. Edgington-Mitchell, An explanation for the phase lag in supersonic jet impingement, J. Fluid Mech. **815**, R1 (2017).
[51] K. Goparaju, Flow and acoustic characterization of complex supersonic Jets, Ph.D. thesis, The Ohio State University, 2017.
[52] S. L. Stahl, C. Prasad, and D. V. Gaitonde, Feedback mechanisms in a supersonic impinging jet using conditional proper orthogonal decomposition, in *AIAA SCITECH 2022 Forum* (AIAA, Reston, VA, 2022).
[53] C. Prasad, S. Stahl, and D. Gaitonde, Exchange mechanisms between hydrodynamic and acoustic components of an under-expanded supersonic impinging jet, in *AIAA Aviation 2021 Forum* (AIAA, Reston, VA, 2021).